338 Vol. 41, No. 2 / February 2024 / Journal of the Optical Society of America A Research Article

Journal of the Optical Society of America A

OPTICS, IMAGE SCIENCE, AND VISION

Fourier reciprocity between generalized elliptical Gaussian and elegant elliptical Hermite-Gaussian beams carrying orbital angular momenta

Davud Hebri,[1,2] Saifollah Rasouli,[1,3,*] and Sergey Ponomarenko[2,4]

[1]Department of Physics, Institute for Advanced Studies in Basic Sciences (IASBS), Zanjan 45137-66731, Iran
[2]Department of Physics and Atmospheric Science, Dalhousie University, Halifax, Nova Scotia B3H 4R2, Canada
[3]Optics Research Center, Institute for Advanced Studies in Basic Sciences (IASBS), Zanjan 45137-66731, Iran
[4]Department of Electrical and Computer Engineering, Dalhousie University, Halifax, Nova Scotia B3J 2X4, Canada
*rasouli@iasbs.ac.ir

Received 23 October 2023; revised 19 December 2023; accepted 24 December 2023; posted 3 January 2024; published 30 January 2024

We explore two distinct families of orbital angular momentum carrying light beams, which we refer to as generalized elliptical Gaussian and elegant elliptical Hermite-Gaussian vortex beams, respectively. We show that the fields of the two vortex families are related via a Fourier transform. Hence, one family can be viewed as a source of the far-field intensity distribution of the other and vice versa. We also examine the orbital angular momentum evolution of both beam families on their free space propagation and establish a relationship between the orbital angular momentum, TC, and beam ellipticity factors. Our results may find applications to optical communications and imaging with structured light.

https://doi.org/10.1364/JOSAA.510096

1. INTRODUCTION

Optical fields with a Laguerre-Gaussian (LG) amplitude distribution, carrying the orbital angular momentum (OAM), have attracted immense interest within the optical community since the pioneering work of Allen *et al.* on the OAM of LG modes [1]. In the last 30 years, OAM has established itself as one of the most interesting of optical modes, with relevance to optical manipulation, imaging, quantum optics, optical communications, and elsewhere [2–4]. Phase singularities and OAM are also characteristic of all optical vortices [5]. Random OAM carrying optical fields have also been studied theoretically [6–8] and experimentally [8,9]. Optical vortices, both coherent and random, have found numerous applications, including neutral particle micromanipulation [10], quantum and classical optical entanglement and teleportation [11–13], super-resolution imaging [3], and free-space optical communications [14].

Generalizations of LG beams have been presented to date. For example, a symbiosis of LG and Hermite-Gaussian (HG) beams has been proposed in [15] and termed Hermite-Laguerre-Gaussian beams by introducing an additional parameter. Adjusting the magnitude of the introduced parameter allows a continuous transition between HG and LG beams, thereby maintaining the salient properties of both beam families. In addition, the transformation of a set of LG modes into a 1D array of HG modes via the Talbot effect has been recently reported [16]. Another extension of LG beams, known as structured Laguerre–Gaussian (sLG) beams, acquires fine structure of their intensity distribution, OAM, and topological charge (TC) [17,18].

Optical vortices with a fractional OAM and without circular symmetry have been intensively studied recently [19]. There are several methods for generating an optical vortex with fractional OAM. For instance, it can be done by off-axis illumination of a spiral phase plate by a Gaussian beam [20,21], or by using a non-integer phase step spiral phase plate [22]. Asymmetric optical vortices with discrete crescent-shape intensity distributions possess fractional orbital angular momenta as well [23–25]. Fractional orbital angular momenta compatible with continuous light intensity distributions in the transverse plane can be realized by generating elliptical vortices [26–30]. To this end, the authors of Ref. [29] introduced the concept of an elliptical Hermite-Gaussian vortex beam and evaluate its OAM. Further, elegant elliptical Hermite–Gaussian (EEHG) vortex beams were originally presented in [31], although their OAM content was not studied. By the same token, elliptical optical vortices embedded into circular Gaussian beams were examined in [30]. Forthwith, a more general case in which both the vortex and the Gaussian beam are elliptical with different ellipticities was discussed in [19] where the authors derived a simple formula for its OAM. Hereafter, we refer to these more general light fields as generalized elliptical Gaussian (GEG) optical vortices.

In this work, we study the GEG and EEHG vortex beam evolution in free space. In particular, we demonstrate that GEG and EEHG vortex sources form a Fourier transform pair. Our results imply that one family can serve as a source for the far-field

vortex intensity distribution given by the other and vice versa. By defining two ellipticity factors for a GEG vortex, say ε_v and ε_g, we show that, if the two factors are equal, the two beam families have identical fields and, hence, are self-Fourier transforms. We also establish that the OAM of any GEG vortex is proportional to its TC and is a function of the ellipticity factors. Since the far-field propagation of an EEHG vortex leads to the generation of a GEG vortex and vice versa, we invoke the OAM conservation on free-space propagation to determine the OAM of an EEHG vortex beam from the knowledge of the GEG beam OAM. We also obtain the EEHG OAM by a direct calculation.

The paper is organized as follows. In Section 2, we introduce GEG and EEHG vortex fields and evaluate the OAM of the GEG field as a function of its TC and the two ellipticity factors. In Sections 3 and 4, we explore the near- and far-field evolution of GEG and EEHG vortex fields, respectively. In Section 5, we consider a particular case when both GEG and EEHG are self-Fourier transforms, followed by our summary in Section 6.

2. GEG AND EEHG OPTICAL VORTICES

Consider a complex amplitude of a conventional optical vortex, which can be written in the Cartesian coordinates as

$$\psi_l(\mathbf{r}) = \left(\frac{x+isy}{w}\right)^{|l|} \exp\left(-\frac{x^2+y^2}{w^2}\right), \tag{1}$$

where $\mathbf{r} = (x, y) = (r\cos\theta, r\sin\theta)$ is a position vector in transverse plane, l is an integer that represents the topological charge (TC) of the vortex, and w is a radial scale parameter such that $w_{\text{eff}} = w\sqrt{|l|/2}$ is an effective beam radius measured from the dark center to the intensity peak of a doughnut-shaped beam. Furthermore, $s = \pm 1$ indicates the TC sign. We now focus on the following generalized form of the optical vortex field:

$$\psi_l(\mathbf{r}) = \left(\frac{x}{a_x} + is\frac{y}{a_y}\right)^{|l|} \exp\left[-\left(\frac{x^2}{w_x^2} + \frac{y^2}{w_y^2}\right)\right], \tag{2}$$

which we hereafter refer to as a generalized elliptical Gaussian (GEG) optical vortex. Here a_x, a_y, w_x, and w_y are transverse length scales determining the ellipticity of the vortex field. Here we define two ellipticity factors $\varepsilon_v = \frac{a_y}{a_x}$ and $\varepsilon_g = \frac{w_y}{w_x}$ for the GEG vortices. We call the first one a vortex ellipticity and the second one a Gaussian ellipticity.

The OAM and the total power of any paraxial light field $\psi_l(x, y)$ can be expressed as [21,23,24]

$$J_z = \text{Im}\int_{-\infty}^{+\infty}\int_{-\infty}^{+\infty} \psi_l^*(\mathbf{r})\left(x\frac{\partial}{\partial y} - y\frac{\partial}{\partial x}\right)\psi_l(\mathbf{r})\,\mathrm{d}x\,\mathrm{d}y, \tag{3}$$

$$W = \int_{-\infty}^{+\infty}\int_{-\infty}^{+\infty} \psi_l^*(\mathbf{r})\psi_l(\mathbf{r})\,\mathrm{d}x\,\mathrm{d}y, \tag{4}$$

where Im stands for the imaginary part of a complex field and $*$ denotes complex conjugation. The normalized OAM of the field, ℓ_z, is defined as the ratio of J_z to W, namely $\ell_z = J_z/W$. It has been shown that substituting from Eq. (2) into Eqs. (3) and (4) results in the normalized OAM in the following form [19]:

$$\ell_z = \frac{J_z}{W} = l\left[\frac{a_x a_y\left(w_y^2 - w_x^2\right)}{a_x^2 w_y^2 - a_y^2 w_x^2} + \frac{w_x w_y\left(a_x^2 - a_y^2\right)}{a_x^2 w_y^2 - a_y^2 w_x^2}\frac{P_{l-1}(\alpha)}{P_l(\alpha)}\right], \tag{5}$$

where $P_l(\alpha)$ is a Legendre polynomial of order l and

$$\alpha = \left(\frac{w_x w_y}{2a_x a_y}\right)\left[\left(\frac{a_x}{w_x}\right)^2 + \left(\frac{a_y}{w_y}\right)^2\right]. \tag{6}$$

It follows that, in sharp contrast to the OAM and TC of a conventional vortex field, defined by Eq. (1), the corresponding quantities for the GEG are not equal to each other, $\ell_z \neq l$. We express the normalized OAM of the GEG as a function of two dimensionless ellipticity factors, ε_v and ε_g, instead of the length parameters a_x, a_y, w_x, and w_y. Therefore, we can cast Eqs. (5) and (6) into the following form:

$$\ell_z = \frac{l}{\varepsilon_g^2 - \varepsilon_v^2}\left[\varepsilon_v\left(\varepsilon_g^2 - 1\right) - \varepsilon_g\left(\varepsilon_v^2 - 1\right)\frac{P_{l-1}(\alpha)}{P_l(\alpha)}\right], \tag{7}$$

$$\alpha = \frac{\varepsilon_g^2 + \varepsilon_v^2}{2\varepsilon_v\varepsilon_g}. \tag{8}$$

We note that Eq. (7) is not directly applicable in the particular case of $\varepsilon_v = \varepsilon_g$. We discuss this case separately in Section 5. Using Eqs. (5) and (7), we determine the ratio of normalized OAM to the TC, ℓ_z/l, as a function of ε_v and ε_g. We exhibit the results in Fig. 1. We can infer from the figure that, depending on the values of ε_v and ε_g, there exist three different cases: $\ell_z/l < 1$, $\ell_z/l > 1$, and $\ell_z/l = 1$, or equivalently $\ell_z < l$, $\ell_z > l$, and $\ell_z = l$.

We now present a concise review of the elegant elliptical Hermite-Gaussian (EEHG) optical vortices, originally introduced in Ref [31]. The complex amplitude of an EEHG vortex field at the source, $z = 0$, can be expressed as

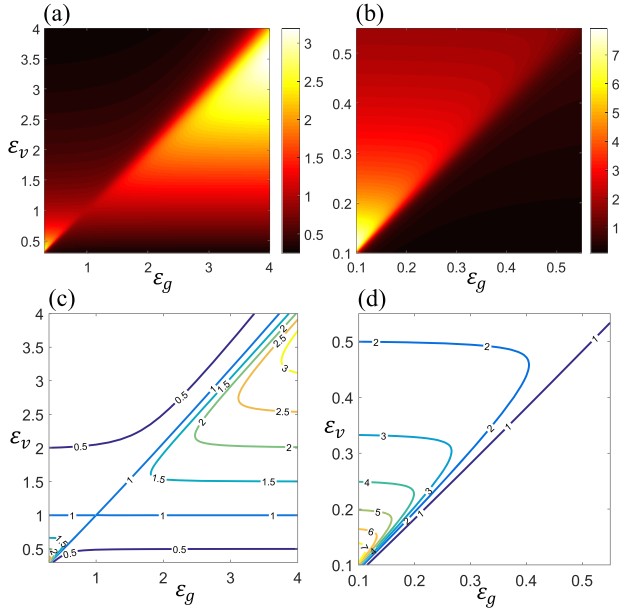

Fig. 1. (a) and (b) Ratio of the normalized OAM to topological charge, ℓ_z/l, in terms of ε_v and ε_g for the GEG optical vortices in two different scales. (c) and (d) The corresponding contour graphs.

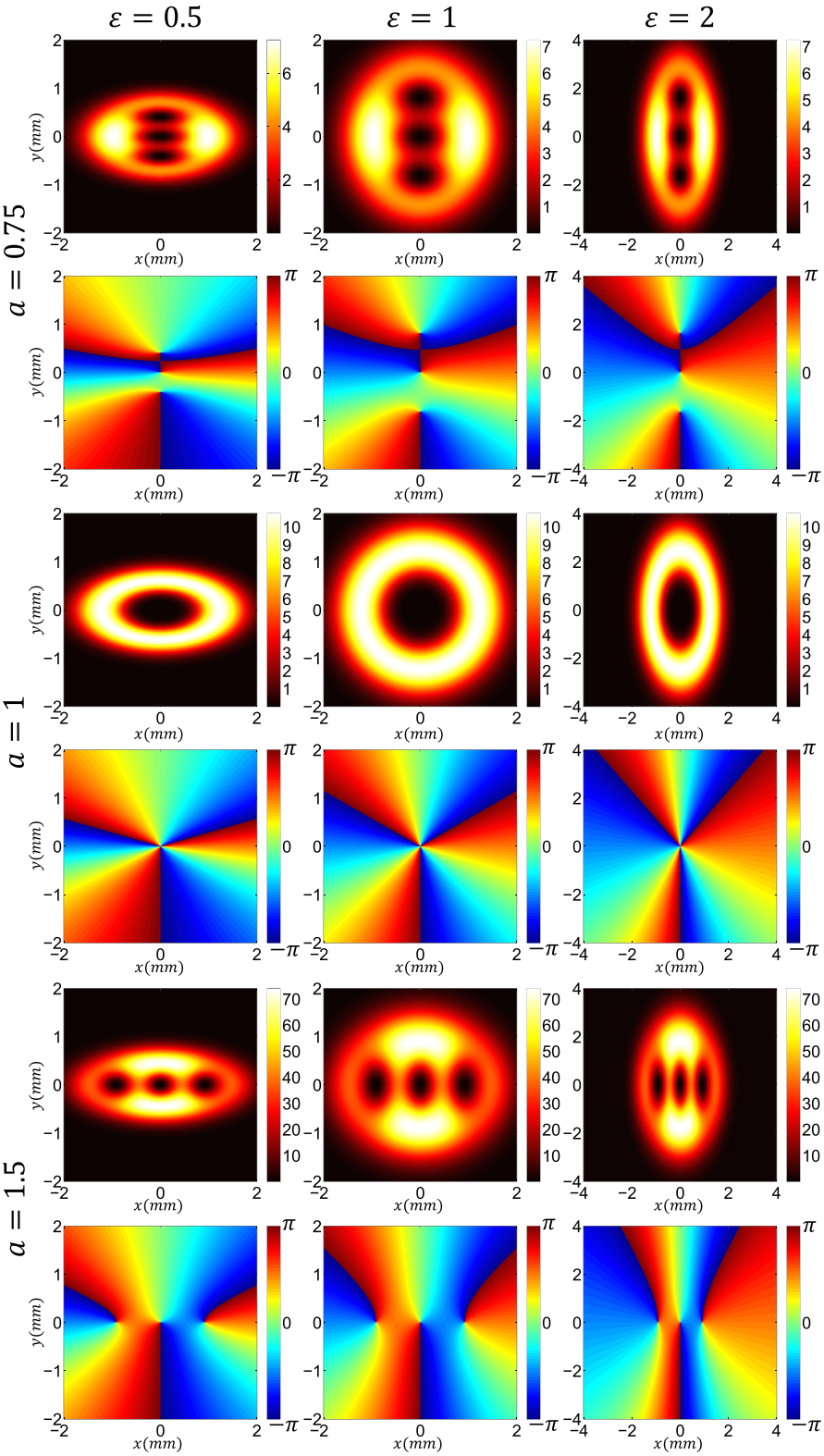

Fig. 2. Intensity (first, third, and fifth rows) and the corresponding phase (second, fourth, and sixth rows) profiles of EEHG vortex fields with $\lambda = 532$ nm, $n = 3$, and $s = +1$ at $z = 0$. The beam waist is fixed at $p_x = 1$ mm, and the parameters a and ε are varied.

$$\psi_n(\mathbf{r}, 0) = e^{-\left(\frac{x^2}{p_x^2}+\frac{y^2}{p_y^2}\right)} \sum_{m=0}^{n} \binom{n}{m} (-isa)^m \times H_m\left(\frac{x}{p_x}\right) H_{n-m}\left(\frac{y}{p_y}\right), \quad (9)$$

which is a linear combination of elegant Hermite Gaussian beams with complex coefficients, where n is the absolute value of topological charge and $s = \pm 1$ indicates its sign. Further,

$\binom{n}{m} = \frac{n!}{m!(n-m)!}$ are binomial coefficients, a is a real positive parameter, and p_x and p_y are the spot sizes of elliptical Gaussian beam waist along the x- and y-axes, respectively. We note that $\varepsilon = \frac{p_y}{p_x}$ can be viewed as the ellipticity factor of an EEHG and the special case of $a = \varepsilon$ was considered in [31]. We show that a and ε are key parameters that characterize the intensity profile and OAM of an EEHG. Under the condition $a \neq 1$, Eq. (9) can be rewritten as

$$\psi_n(\mathbf{r}, 0) = \left(1 - a^2\right)^{n/2} \exp\left[-\left(\frac{x^2}{p_x^2} + \frac{y^2}{p_y^2}\right)\right] \times H_n\left[\frac{-is\,a\,(x/p_x) + (y/p_y)}{\sqrt{1-a^2}}\right], \tag{10}$$

with the help of Eq. (A2). We discuss the special case $a = 1$ in Section 5. In Fig. 2, we display the intensity and phase profiles of an EEHG vortex field with $p_x = 1$ mm for different values of a and ε in the source plane $z = 0$. The parameters a and ε strongly affect the intensity and phase profiles of the EEHG. The intensity profile is a horizontal ellipse when $\varepsilon < 1$ and a vertical ellipse when $\varepsilon > 1$. Whenever $\varepsilon = 1$, the ellipse orientation depends on a as we show in the second column of Fig. 2. The parameter a is also crucial—it determines the number and location of the intensity nulls. As long as $a < 1$ and $a > 1$, there are n nulls with TC $= s$ on the y axis and x axis, respectively. Provided $a = 1$, all nulls merge into one at the origin, corresponding to TC $= s\,n$.

3. NEAR- AND FAR-FIELD PROPAGATION OF GEG OPTICAL VORTICES

First, we examine the evolution of GEG optical vortices in free space in the near-field regime. Considering $\psi(\mathbf{r}', 0)$ as the complex amplitude of a paraxial, quasi-monochromatic optical field at $z = 0$, the complex amplitude of the field in any transverse plane $z = \text{const} \geq 0$ is, in general, given by the Fresnel integral:

$$\psi(\mathbf{r}, z) = h \int_{-\infty}^{\infty}\int_{-\infty}^{\infty} \psi(\mathbf{r}', 0) e^{i\alpha\left[x'^2 + y'^2 - 2(xx' + yy')\right]} \mathrm{d}x'\mathrm{d}y', \tag{11}$$

where $\alpha = \frac{\pi}{z\lambda}$, λ is the wavelength of light, and

$$h = \frac{1}{i\lambda z} \exp\left(ikz + i\alpha r^2\right), \tag{12}$$

where $k = \frac{2\pi}{\lambda}$ is a wavenumber, and $r = \sqrt{x^2 + y^2}$ is radial distance from the z-axis. Employing the binomial expansion, the complex amplitude of a GEG vortex beam at $z = 0$, given by Eq. (2), can be transformed to

$$\psi_l(\mathbf{r}, 0) = \left(\frac{i}{a_y}\right)^{|l|} e^{-\left(\frac{x^2}{w_x^2} + \frac{y^2}{w_y^2}\right)} \sum_{m=0}^{|l|} \binom{|l|}{m} (-is\,\varepsilon_v)^m x^m y^{|l|-m}, \tag{13}$$

where $\varepsilon_v = \frac{a_y}{a_x}$. On substituting this complex amplitude into Eq. (11), and using the following reference integral [32],

$$\int_{-\infty}^{+\infty} u^m e^{-(Au^2 + Bu)} \mathrm{d}u = \sqrt{\pi}\left(\frac{i}{2}\right)^m A^{-(m+1)/2} e^{B^2/(4A)} H_m\left(\frac{iB}{2\sqrt{A}}\right), \tag{14}$$

and introducing

$$\frac{1}{\beta_x^2} = \frac{1}{w_x^2} - i\frac{\pi}{z\lambda} = \frac{1}{w_x^2}\left(1 - i\frac{z_{0x}}{z}\right), \tag{15a}$$

$$\frac{1}{\beta_y^2} = \frac{1}{w_y^2} - i\frac{\pi}{z\lambda} = \frac{1}{w_y^2}\left(1 - i\frac{z_{0y}}{z}\right), \tag{15b}$$

we obtain the expression

$$\psi_l(\mathbf{r}, z) = c_l e^{-\alpha^2\left(\beta_x^2 x^2 + \beta_y^2 y^2\right)} \sum_{m=0}^{|l|} \binom{|l|}{m} (-is\,a(z))^m \times H_m(\alpha\beta_x x)\, H_{|l|-m}\left(\alpha\beta_y y\right). \tag{16}$$

Here, $c_l = \pi h \left(\frac{s\beta_y}{2a_y}\right)^{|l|} \beta_x\beta_y$, $a(z) = \frac{a_y\beta_x}{a_x\beta_y}$. Further, $z_{0x} = \frac{\pi w_x^2}{\lambda}$ and $z_{0y} = \frac{\pi w_y^2}{\lambda}$ are the Rayleigh lengths associated with the transverse confinement along the x and y axes, respectively, and $z_0 = \max\{z_{0x}, z_{0y}\}$ is an effective Rayleigh length. We define the latter as a distance from the beam waist plane over which the beam radius increases by the factor of $\sqrt{2}$. With the aid of Eq. (A2), Eq. (16) can be rewritten in a closed form as

$$\psi_l(\mathbf{r}, z) = c_l\left(1 - a^2(z)\right)^{|l|/2} e^{-\alpha^2\left(\beta_x^2 x^2 + \beta_y^2 y^2\right)} \times H_{|l|}\left[\frac{-is\,a(z)\alpha\beta_x x + \alpha\beta_y y}{\sqrt{1 - a^2(z)}}\right]. \tag{17}$$

The first and second rows of Fig. 3 respectively show the intensity and phase profiles of the GEG beams having $\lambda = 532$ nm, $l = 3$, $w_x = a_x = 0.2$ mm, and different ellipticity factors at $z = 0$. We exhibit the near-field evolution of these beams at $z = 50$ cm in the third and fourth rows of the figure. It can be inferred from the figure that the central dark notch splits into a few secondary ones with unit topological charges so that the number of secondary notches equals the topological charge of the source GEG vortex (see Visualization 1, Visualization 2, Visualization 3, Visualization 4, Visualization 5, and Visualization 6).

Next, we study the far-field propagation properties of the field. As z is increased to the point such that $\frac{\pi(x'^2 + y'^2)_{\max}}{\lambda z} \ll 1$, the term $\alpha(x'^2 + y'^2)$ can be ignored in Eq. (11), leading to

$$\psi(\mathbf{r}, z) = h\tilde{\psi}\left(\frac{x}{\lambda z}, \frac{y}{\lambda z}, 0\right) = h\int_{-\infty}^{+\infty}\int_{-\infty}^{+\infty} \psi(\mathbf{r}', 0) e^{-2i\alpha(xx' + yy')} \mathrm{d}x'\mathrm{d}y', \tag{18}$$

where $\tilde{\psi}(\xi, \eta, 0)$ denotes the Fourier transform of $\psi(x, y, 0)$ or the spatial spectrum of the complex amplitude distribution at the input plane. We note in passing that sometimes h is replaced

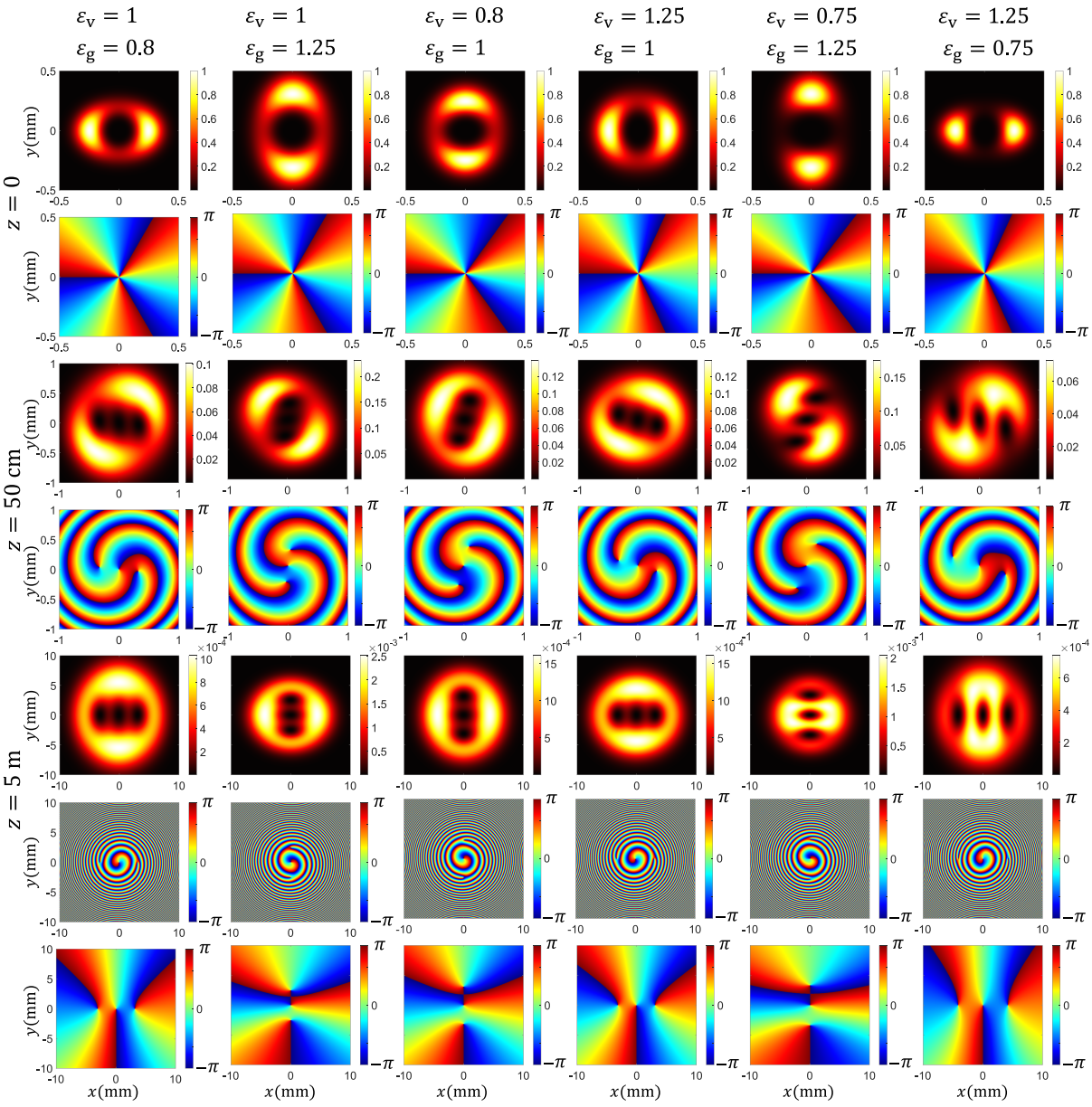

Fig. 3. Near- and far-field evolution of GEG beams with $\lambda = 532$ nm, $l = 3$, $w_x = a_x = 0.2$ mm, and different ellipticity factors. The first, third, and fifth rows show intensity profiles, and the second, fourth, and sixth rows illustrate the corresponding phase profiles. The seventh row exhibits the same profiles as the sixth row, where we dropped the overall phase factor h (see also Visualization 1, Visualization 2, Visualization 3, Visualization 4, Visualization 5, and Visualization 6).

by $h_0 = \frac{\exp(ikz)}{i\lambda z}$ in Eq. (18) by neglecting the quadratic phase $\exp(i\alpha r^2)$ in Eq. (12). This approximation is only justified if we limit our interest to the points in the observation plane within a circle of radius R centered around the z-axis so that $\alpha R^2 = \frac{\pi R^2}{\lambda z} \ll 1$ [33,34]. On the other hand, the size of a diffracted light beam in the far-field region increases roughly linearly with z, comparing capture sizes in different rows of Fig. 3 and also Fig. 4. Therefore, the condition $\frac{\pi R^2}{\lambda z} \ll 1$ can break down for sufficiently large z, and replacing h with h_0 is no longer justified. This approximation can then lead to the erroneous conclusion that "the complex amplitude of a diffracted wave field in the far zone of the source is simply proportional to the Fourier transform of the field amplitude at the source." Strictly speaking, only the far-zone intensity distribution is proportional to the square of the absolute value of the Fourier transform of complex amplitude distribution at the source plane.

On substituting from Eq. (13) into Eq. (18) and using Eq. (14), we arrive at

$$\psi_l(\mathbf{r}, z) = c_l e^{-\alpha^2\left(w_x^2 x^2 + w_y^2 y^2\right)} \sum_{m=0}^{|l|} \binom{|l|}{m} (-is\,a)^m \times H_m(\alpha w_x x)\, H_{|l|-m}\left(\alpha w_y y\right), \tag{19}$$

where $c_l = \pi h (\frac{s\,w_y}{2a_y})^{|l|} w_x w_y$ and $a = \frac{\varepsilon_v}{\varepsilon_g}$. For the case $\varepsilon_v \neq \varepsilon_g$ ($a \neq 1$), we can employ Eq. (A2) to reduce Eq. (19) to

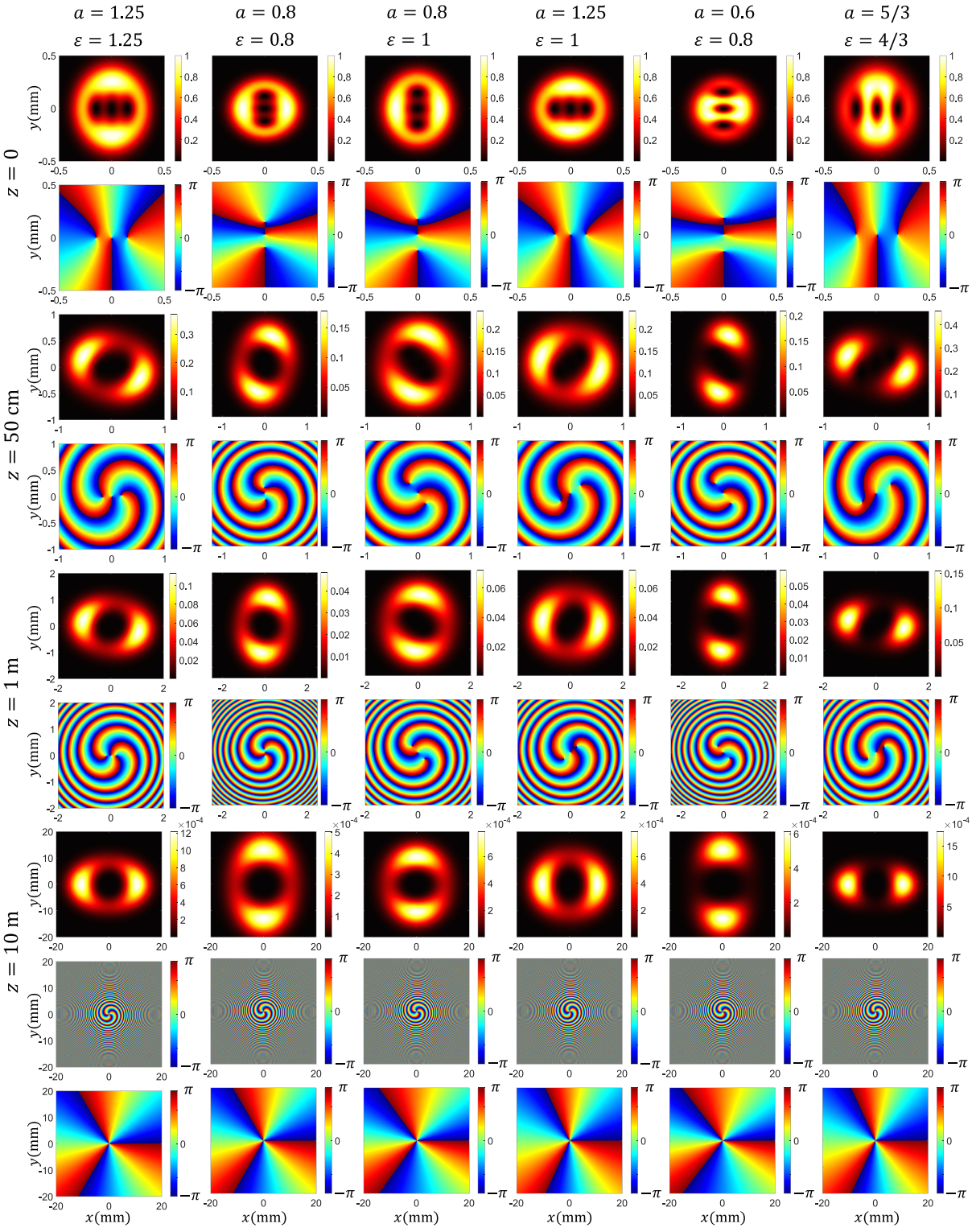

Fig. 4. Near- and far-field evolution of EEHG fields with $\lambda = 532$ nm, $n = 3$, $s = +1$, and $p_x = 0.2$ mm for different parameter values: a and ε. The first, third, fifth, and seventh rows show intensity profiles, and the second, fourth, sixth, and eighth rows exhibit the corresponding phase profiles. The ninth row shows the same profiles as those in the eighth row if we drop the phase factor h.

$$\psi_l(\mathbf{r}, z) = c_l\left(1 - a^2\right)^{|l|/2} e^{-\alpha^2\left(w_x^2 x^2 + w_y^2 y^2\right)} \times H_{|l|}\left[\frac{-ias\alpha w_x x + \alpha w_y y}{\sqrt{1 - a^2}}\right]. \quad (20)$$

In the far-field region, where $z \gg z_0 = \max\{z_{0x}, z_{0y}\}$, Eq. (15) simplifies to $\beta_x = w_x$ and $\beta_y = w_y$. By substituting these values in Eqs. (16) and (17), we can obtain Eqs. (19) and (20) without doing the integral in Eq. (18).

We relegate the special case $\varepsilon_v = \varepsilon_g$ $(a = 1)$ to Section 5. Comparing Eqs. (19) and (9) or equivalently Eqs. (20) and (9) shows that the Fourier transform of a GEG optical vortex leads to an EEHG optical vortex with the characteristic parameters $\varepsilon = \frac{1}{\varepsilon_g}$ and $a = \frac{\varepsilon_v}{\varepsilon_g}$. Using Eq. (20), intensity and phase profiles in the far-field region, $z = 5$ m, are illustrated in the fifth and sixth rows of Fig. 3, respectively. For checking out the Fourier connection between GEG and EEHG optical vortices, compare the fifth and seventh rows of Fig. 3 with the first and second rows of Fig. 4, respectively.

At this point, we would like to caution against a potential pitfall. As one of the introduced beam families, GEG, say, transforms into the other over a long—on the wavelength scale—propagation distance, one might wonder whether the resulting EEHG family can then transform back into the GEG one over another long propagation stretch in the same direction. This, of course, is not true. The mathematical reason for this can be traced to Eqs. (9) and (19). On comparing the two equations, we can conclude that the complex amplitude distribution of a GEG beam in the far zone is the same as that of an EEHG vortex beam at the source *only* up to the phase factor h. The phase factor carries information of the propagation length and the coordinates of the observation plane via Eq. (12), which rules out repeated generation of one vortex family from the other by propagation ad infinitum.

4. NEAR- AND FAR-FIELD PROPAGATION OF EEHG VORTEX BEAMS

On substituting from Eq. (9) into Eq. (11), the near-field evolution of an EEHG vortex beam is governed by the integral

$$\psi_n(\mathbf{r}, z) = h \sum_{m=0}^{n} \binom{n}{m} (-is\,a)^m \times \int_{-\infty}^{+\infty} e^{-\left(\frac{x'}{q_x}\right)^2 - 2i\alpha x x'} H_m\left(\frac{x'}{p_x}\right) \mathrm{d}x' \times \int_{-\infty}^{+\infty} e^{-\left(\frac{y'}{q_y}\right)^2 - 2i\alpha y y'} H_{n-m}\left(\frac{y'}{p_y}\right) \mathrm{d}y', \quad (21)$$

where

$$\frac{1}{q_x^2} = \frac{1}{p_x^2} - i\frac{\pi}{z\lambda} = \frac{1}{p_x^2}\left(1 - i\frac{z_{0x}}{z}\right), \quad (22a)$$

$$\frac{1}{q_y^2} = \frac{1}{p_y^2} - i\frac{\pi}{z\lambda} = \frac{1}{p_y^2}\left(1 - i\frac{z_{0y}}{z}\right). \quad (22b)$$

By defining the following dimensionless parameters: $X' = \frac{x'}{q_x}$, $Y' = \frac{y'}{q_y}$, $X = -i\alpha q_x x$, $Y = -i\alpha q_y y$, $\gamma_x = \frac{q_x}{p_x}$, and $\gamma_y = \frac{q_y}{p_y}$, Eq. (21) reduces to

$$\psi_n(\mathbf{r}, z) = h q_x q_y e^{(X^2+Y^2)} \sum_{m=0}^{n} \binom{n}{m} (-is\,a)^m \times \int_{-\infty}^{+\infty} \mathrm{d}X' e^{-(X'-X)^2} H_m(\gamma_x X') \times \int_{-\infty}^{+\infty} \mathrm{d}Y' e^{-(Y'-Y)^2} H_{n-m}(\gamma_y Y'). \quad (23)$$

Now using the following reference integral [32]:

$$\int_{-\infty}^{+\infty} e^{-(x'-x)^2} H_n(\gamma x')\mathrm{d}x' = \sqrt{\pi}\left(1-\gamma^2\right)^{\frac{n}{2}} H_n\left(\frac{\gamma x}{\sqrt{1-\gamma^2}}\right), \quad (24)$$

we obtain the expression

$$\psi_n(\mathbf{r}, z) = h\pi q_x q_y \left(1-\gamma_y^2\right)^{\frac{n}{2}} e^{X^2+Y^2} \sum_{m=0}^{n} \binom{n}{m} (-is\,\gamma)^m \times H_m\left(\frac{\gamma_x X}{\sqrt{1-\gamma_x^2}}\right) H_{n-m}\left(\frac{\gamma_y Y}{\sqrt{1-\gamma_y^2}}\right), \quad (25)$$

where $\gamma = a\sqrt{\frac{1-\gamma_x^2}{1-\gamma_y^2}}$. Here again by defining $\xi = \frac{\gamma_x X}{\sqrt{1-\gamma_x^2}}$ and $\eta = \frac{\gamma_y Y}{\sqrt{1-\gamma_y^2}}$ and using Eq. (A2), Eq. (25) can be rewritten as follows:

$$\psi_n(\mathbf{r}, z) = h\pi q_x q_y \left[\left(1-\gamma_y^2\right) - a^2\left(1-\gamma_x^2\right)\right]^{n/2} e^{X^2+Y^2} \times H_n\left(\frac{-is\,\gamma\xi + \eta}{\sqrt{1-\gamma^2}}\right). \quad (26)$$

The first and second rows of Fig. 4 show the intensity and phase profiles of the EEHG beams with $n = 3$, $s = +1$, and $p_x = 0.2$ mm at the source, $z = 0$, as the values of a and ε are varied. We visualize the near-field evolution of these beams at $z = 50$ cm and $z = 1$ m in the third to sixth rows of the figure.

We can obtain the far-field distribution of an EEHG vortex beam by substituting from Eq. (9) into Eq. (18). By defining the following dimensionless parameters: $X = -i\alpha p_x x$, $Y = -i\alpha p_y y$, $X' = \frac{x'}{p_x}$, and $Y' = \frac{y'}{p_y}$, the result can be expressed as

$$\psi_n(\mathbf{r}, z) = h p_x p_y e^{(X^2+Y^2)} \times \sum_{m=0}^{n} (-is\,a)^m \binom{n}{m} \times \int_{-\infty}^{\infty} \mathrm{d}X' e^{-(X'-X)^2} H_m(X') \times \int_{-\infty}^{\infty} \mathrm{d}Y' e^{-(Y'-Y)^2} H_{n-m}(Y'). \quad (27)$$

Using the following reference integral [32]:

$$\int_{-\infty}^{\infty} e^{-(x'-x)^2} H_n(x')\mathrm{d}x' = \sqrt{\pi}2^n x^n, \tag{28}$$

Eq. (28) leads to

$$\psi_n(\mathbf{r}, z) = 2^n \pi\, p_x p_y h e^{(X^2+Y^2)} \sum_{m=0}^{n} \binom{n}{m} (-is\,a\,X)^m Y^{n-m}. \tag{29}$$

Now invoking Newton's binomial expansion, we arrive at

$$\psi_n(\mathbf{r}, z) = h\pi\, p_x p_y (-2is\,a)^n (X + iY/a)^n e^{X^2+Y^2}, \tag{30}$$

and consequently

$$\psi_n(\mathbf{r}, z) = A_n (ax + is\varepsilon y)^n e^{-\alpha^2\left(p_x^2x^2+p_y^2y^2\right)}, \tag{31}$$

where $A_n = h\pi\, p_x p_y (-2is\alpha p_x)^n$ and $\varepsilon = \frac{p_y}{p_x}$. Comparing Eq. (31) and the general form of GEG vortices, Eq. (2), we can conclude that the far-field intensity distribution of an EEHG vortex is identical to the GEG vortex intensity at the source, provided the ellipticity factors are identified as $\varepsilon_v = \frac{a}{\varepsilon}$ and $\varepsilon_g = \frac{1}{\varepsilon}$. This feature can be verified by comparing the seventh row of Fig. 4 with the first row of Fig. 3. Further, by comparing the ninth row of Fig. 4 and the second row of Fig. 3, Fourier reciprocity between EEHG and GEG vortices can be observed.

It follows that, by applying the OAM and power conservation on free-space propagation [35], the normalized OAM of any EEHG vortex beam can be obtained by substituting $\varepsilon_v = \frac{a}{\varepsilon}$ and $\varepsilon_g = \frac{1}{\varepsilon}$ into Eq. (7). The result reads

$$\ell_z = \frac{n}{\varepsilon\left(1-a^2\right)}\left[a\left(1-\varepsilon^2\right) - \left(a^2-\varepsilon^2\right)\frac{P_{n-1}(\alpha)}{P_n(\alpha)}\right], \tag{32}$$

where $\alpha = \frac{1+a^2}{2a}$. We should mention that Eq. (32) breaks down in the special case of $a = 1$ which we discuss separately in the following section. Using Eqs. (32) and (34), we can work out the ratio of the normalized OAM to topological charge ℓ_z/n as a function of ε and a. We depict the results graphically in Fig. 5. As is seen in the figure, $\ell_z/n = 1$ for $\varepsilon = a$, and hence the normalized OAM is equal to the topological charge of the EEHG vortex beam. The generation of this class of EEHG vortex beams with $\varepsilon = a$ has already been discussed in [31] by considering the diffraction of a conventional vortex beam from an elliptical aperture.

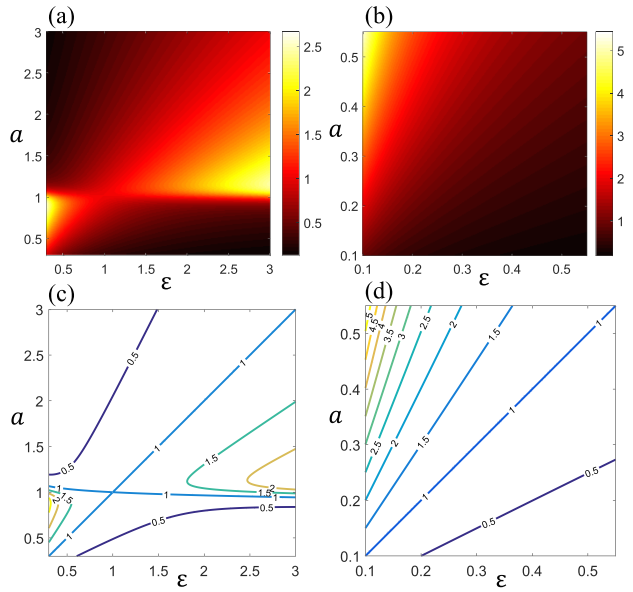

Fig. 5. (a) and (b) Ratio of the normalized OAM to topological charge, ℓ_z/n in terms of ε and a for EEHG vortex beams using two different scales. (c) and (d) The corresponding contour graphs.

5. FOURIER-INVARIANT GEG AND EEHG VORTEX BEAMS

Let us now focus on the particular case of GEGs with equal ellipticity factors, $\varepsilon_v = \varepsilon_g = \varepsilon$. In this case, we can rewrite Eq. (2) as

$$\psi_l(\mathbf{r}) = \left(\frac{x}{w_x} + is\frac{y}{w_y}\right)^{|l|} e^{-\left(\frac{x^2}{w_x^2}+\frac{y^2}{w_y^2}\right)}, \tag{33}$$

It follows that the evaluation of ℓ_z with the aid of Eq. (7) leads to uncertainty, as both the numerator and denominator approach zero. Resolving the uncertainty, we obtain

$$\ell_z = l\left(\frac{\varepsilon + \varepsilon^{-1}}{2}\right), \tag{34}$$

where $\varepsilon = \frac{w_y}{w_x}$; see Eq. (12) of Ref. [19]. The near-field evolution of an ellipticity-matched GEG can then be obtained from Eqs. (16) or (17) by taking $c_l = \pi h(\frac{s\beta_y}{2w_y})^l \beta_x \beta_y$ and $a(z) = \varepsilon\frac{\beta_x}{\beta_y}$. By the same token, we can determine the far-field distribution of an ellipticity-matched GEG from Eq. (16) by setting $a = 1$. Considering Eq. (A5), Eq. (19) for the ellipticity-matched GEG reduces to

$$\psi_l(\mathbf{r}, z) = \pi h w_x w_y (-i)^{|l|}\left(\alpha w_x x + is\alpha w_y y\right)^{|l|} e^{-\alpha^2\left(w_x^2x^2+w_y^2y^2\right)}, \tag{35}$$

We display near- and far-field evolution of Fourier-invariant GEG beams with $\lambda = 532$ nm, $l = 3$, $w_x = 0.2$ mm, and different ellipticity factors in Fig. 6. We can infer from the figure that the far-field distribution of the ellipticity-matched GEG is Fourier invariant up to a 90-deg rotation, which corresponds to the inverted ellipticity factor, $\varepsilon' = 1/\varepsilon$. We can verify this feature by comparing the intensity profiles in the first row of the figure, reading from left to right, with those in the fifth row, reading from right to left. As well, we can compare the phase profiles in rows two and seven.

We now turn to the EEHG vortex beams in the special case $a = 1$. On substituting $a = 1$ into Eq. (9) and using Eq. (A5), we obtain

$$\psi_n(\mathbf{r}, 0) = (-2i)^n\left(\frac{x}{p_x} + is\frac{y}{p_y}\right)^n e^{-\left(\frac{x^2}{p_x^2}+\frac{y^2}{p_y^2}\right)}, \tag{36}$$

which is an ellipticity-matched GEG. In other words, when $a = 1$, an EEHG vortex beam and an ellipticity-matched GEG are the same, and both of them are Fourier invariant. Therefore, on taking $\varepsilon = \frac{p_y}{p_x}$, we can obtain their normalized OAM with the aid of Eq. (35).

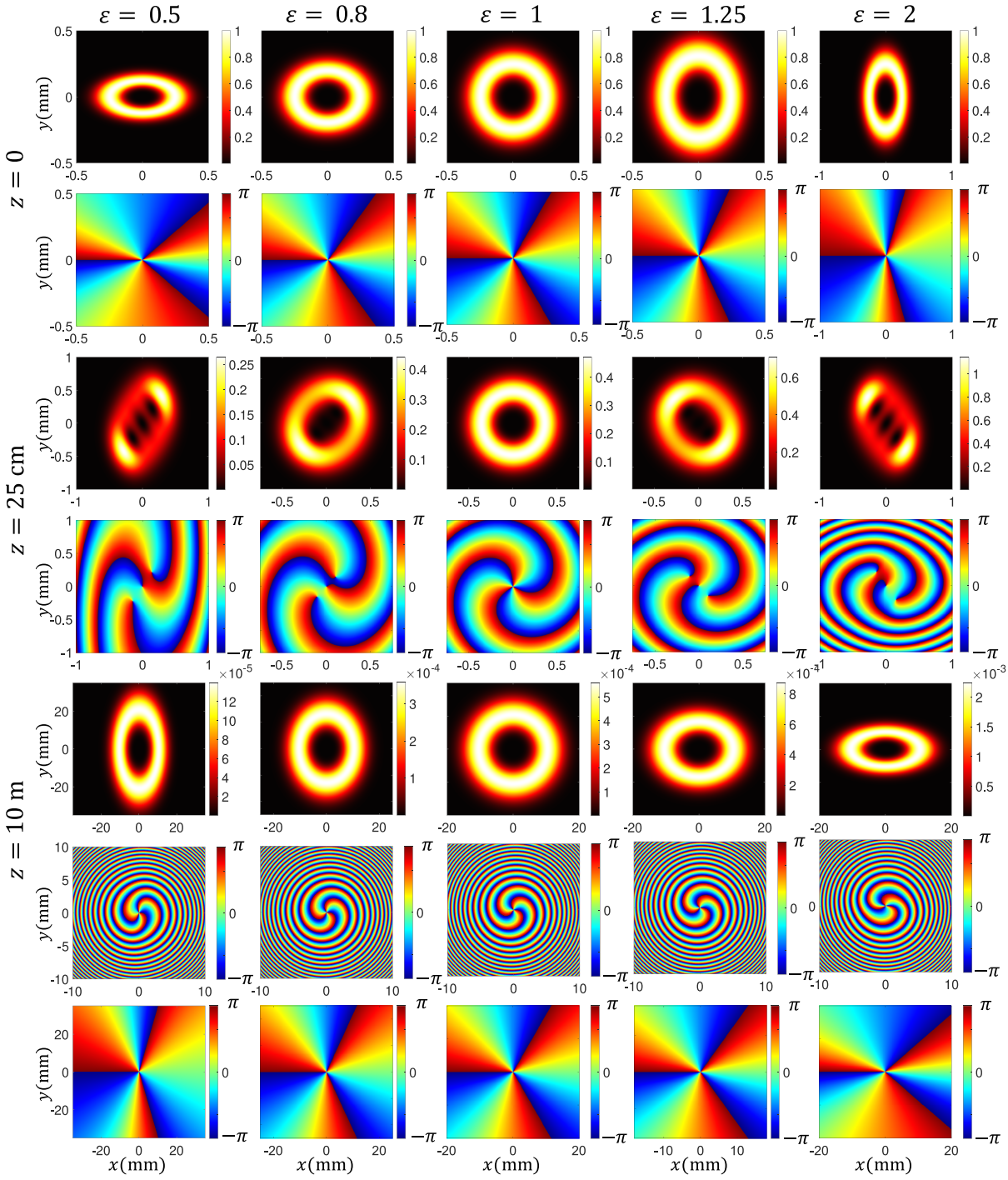

Fig. 6. Near- and far-field evolution of Fourier-invariant GEG vortex beams with $\lambda = 532$ nm, $l = 3$, $w_x = 0.2$ mm, and different ellipticity factors. The first, third, and fifth rows show intensity profiles, and the second, fourth, and sixth rows illustrate the corresponding phase profiles. The seventh row exhibits the same profiles as the sixth row, where we dropped the overall phase factor h.

6. SUMMARY

We have explored the near-field evolution in free space and far-field distribution of two families of optical vortex beams, generalized elliptical Gaussian (GEG) and elegant elliptical Hermite-Gaussian (EEHG). We have established a reciprocity relation between the source and far-field distributions of the fields of GEG and EEHG beam families. In particular, we have shown that the source field distribution of one family is related to the far-field distribution of the other by a Fourier transform. Using the Fourier reciprocity of the GEG and EEHG vortex beams, we have evaluated their orbital angular momenta. We compared our evaluation with a direct method. We have found a condition for the fields of the two beam families to become Fourier-invariant. Our results may find applications to optical

communications and imaging with structured light. In particular, our work informs the transformation of GEG beams with different orbital angular momenta and ellipticities into EEHG beams with the same orbital angular momenta and different ellipticities, thereby introducing novel beam shapes. Therefore, these beams can be employed for information encoding and decoding in optical fibers, or for contrast or resolution enhancement in optical microscopy.

APPENDIX A

Consider a Hermite polynomial of degree n, $H_n(x)$. We can represent the polynomial as $H_n(x) = (2x)^n$ for $n < 2$ and $H_n(x) = (2x)^n + \mathrm{O}(x)^{n-2}$ for $n \geq 2$, where $\mathrm{O}(x)^{n-2}$ denotes a polynomial of degree $n-2$. Further, considering α to be a nonzero real variable, we have $\alpha^n H_n(\frac{x}{\alpha}) = (2x)^n$, provided $n < 2$, and $\alpha^n H_n(\frac{x}{\alpha}) = (2x)^n + \alpha^n \mathrm{O}(\frac{x}{\alpha})^{n-2}$ for $n \geq 2$, where $\mathrm{O}(\frac{x}{\alpha})^{n-2}$ denotes a polynomial of $(\frac{x}{\alpha})$ of degree $n-2$. We can then examine the behavior of $\alpha^n H_n(\frac{x}{\alpha})$ in the limit $\alpha \to 0$. It follows that

$$\lim_{\alpha \to 0} \alpha^n H_n\left(\frac{x}{\alpha}\right) = (2x)^n. \tag{A1}$$

Let us now recall the identity [29]

$$\sum_{m=0}^{n} t^m \binom{n}{m} H_m(\xi) H_{n-m}(\eta) = \left(1+t^2\right)^{\frac{n}{2}} H_n\left(\frac{t\xi+\eta}{\sqrt{1+t^2}}\right). \tag{A2}$$

In the particular case of $t = \mp i$, we must evaluate both sides of Eq. (A2) in the limit $t \to \mp i$. The left-hand side then reads

$$\sum_{m=0}^{n} (\mp i)^q \binom{n}{m} H_m(\xi) H_{n-m}(\eta), \tag{A3}$$

whereas the right-hand side can be calculated by defining $\alpha = \sqrt{1+t^2}$ and $\chi = \mp i\xi + \eta = \mp i(\xi \pm i\eta)$, and using Eq. (A1). The result is

$$\lim_{t \to \mp i} \left(1+t^2\right)^{\frac{n}{2}} H_n\left(\frac{t\xi+\eta}{\sqrt{1+t^2}}\right) = \lim_{\alpha \to 0} \alpha^n H_n\left(\frac{\chi}{\alpha}\right) = 2^n \chi^n = (\mp 2i)^n (\xi \pm i\eta)^n. \tag{A4}$$

We have thus proven the following identity:

$$\sum_{m=0}^{n} (\mp i)^m \binom{n}{m} H_m(\xi) H_{n-m}(\eta) = (\mp 2i)^n (\xi \pm i\eta)^n. \tag{A5}$$

APPENDIX B

We now derive a general expression for the normalized OAM of any EEHG vortex beam by performing the integration in Eqs. (3) and (4). On substituting the expression for ψ_n from Eq. (9) into Eqs. (3) and (4), the OAM and power of an EEHG vortex beam can be calculated. To this end, we require the following integral [32]:

$$\int_{-\infty}^{\infty} e^{-2x^2} H_m(x) H_n(x) \mathrm{d}x = \begin{cases} 0, & m+n = \text{odd}, \\ (-1)^{\lfloor m/2 \rfloor + \lfloor n/2 \rfloor} 2^{\frac{m+n-1}{2}} \Gamma\left(\frac{m+n+1}{2}\right), & m+n = \text{even}, \end{cases} \tag{B1}$$

where m and n are positive integers, $\lfloor\ \rfloor$ denotes an integer part function, and Γ stands for a gamma function. Defining $\varepsilon(m, n)$ as

$$\varepsilon(m, n) = \begin{cases} +1, & \text{both of } m \text{ and } n \text{ are even}, \\ -1, & \text{both of } m \text{ and } n \text{ are odd}, \\ 0, & \text{otherwise}. \end{cases} \tag{B2}$$

Equation (B1) can be rewritten as follows:

$$\int_{-\infty}^{\infty} e^{-2x^2} H_m(x) H_n(x) \mathrm{d}x = \varepsilon(m, n) (-1)^{\lfloor \frac{m+n}{2} \rfloor} 2^{\frac{m+n-1}{2}} \Gamma\left(\frac{m+n+1}{2}\right). \tag{B3}$$

Integrating by parts on the left-hand side of Eq. (B3), we obtain

$$\int_{-\infty}^{\infty} x e^{-2x^2} H_m(x) H_n(x) \mathrm{d}x = \tilde{\varepsilon}(m, n) \frac{(m-n)}{4} (-1)^{\lfloor \frac{m+n}{2} \rfloor} 2^{\frac{m+n}{2}} \Gamma\left(\frac{m+n}{2}\right), \tag{B4}$$

where $\tilde{\varepsilon}(m, n)$ is defined as

$$\tilde{\varepsilon}(m, n) = \begin{cases} +1, & m \text{ is odd and } n \text{ is even}, \\ -1, & m \text{ is even and } n \text{ is odd}, \\ 0, & \text{otherwise}. \end{cases} \tag{B5}$$

On substituting from Eq. (B3) into Eq. (4), we find that the power of the EEHG vortex beam is given by the following expression:

$$W = 2^{n-1} \left(1+a^2\right)^{-n/2} p_x p_y \sum_{p=0}^{n} \sum_{q=0}^{n} a^{p+q} W_{p,q}, \tag{B6}$$

where

$$W_{p,q} = |\varepsilon(p, q)| (-1)^{\frac{p-q}{2}} \binom{n}{p} \binom{n}{q} \times \Gamma\left(\frac{2n-p-q+1}{2}\right) \Gamma\left(\frac{p+q+1}{2}\right). \tag{B7}$$

Next, writing the OAM as $J_z = \mathrm{Im}\{\tilde{J}_z\}$ and using Eqs. (B4) and (B5), the following relation can be derived:

$$\tilde{J}_z = s_n \{(\varepsilon - \varepsilon^{-1}) \sum_{p=0}^{n} \sum_{q=0}^{n} (p-q) J_{p,q} - 2\varepsilon^{-1} \sum_{p=0}^{n-1} \sum_{q=0}^{n} (n-p) J_{p,q} - 2\varepsilon \sum_{p=1}^{n} \sum_{q=0}^{n} p J_{p,q}\}. \tag{B8}$$

Here,

$$s_n = \frac{2^n}{8}\left(1+a^2\right)^{-n/2} p_x p_y,$$

$$J_{p,q} = |\tilde{\varepsilon}(p,q)|\, a^{p+q} (i)^{p-q} \binom{n}{p}\binom{n}{q} (p-q)\Gamma_{p,q},$$

where $\Gamma_{p,q} = \Gamma(\frac{p+q}{2})\Gamma(n-\frac{p+q}{2})$. Finally, using these results, one can obtain the OAM of an EEHG vortex beam as a function of ε and a parameters. For the power-independent OAM of the EEHG vortex beam, for instance, the normalized OAM of the beam can be evaluated as

$$\ell_z = \frac{\mathrm{Im}\{\tilde{J}_z\}}{W}, \tag{B9}$$

where W and $\tilde{J}_z$ are obtained from Eqs. (B7) and (B8).

Funding. Iran National Science Foundation (4020609); Institute for Advanced Studies in Basic Sciences (G2023IASBS12632); Natural Sciences and Engineering Research Council of Canada (RGPIN-2018-05497).

Acknowledgment. This work is based upon research funded by Institute for Advanced Studies in Basic Sciences and by Iran National Science Foundation (INSF). The author Saifollah Rasouli would like to acknowledge support from the ICTP through the Associates Programme. The author Davud Hebri would like to acknowledge Izaak Walton Killam Postdoctoral fellowship. The authors Davud Hebri and Sergey Ponomarenko acknowledge financial support from the Natural Sciences and Engineering Research Council of Canada and Izaak Walton Killam Postdoctoral fellowship.

Disclosures. The authors declare no conflicts of interest.

Data availability. No data were generated or analyzed in the presented research.

REFERENCES

1. L. Allen, M. W. Beijersbergen, R. Spreeuw, *et al.*, "Orbital angular momentum of light and the transformation of Laguerre-Gaussian laser modes," Phys. Rev. A **45**, 8185–8189 (1992).
2. M. J. Padgett, "Orbital angular momentum 25 years on," Opt. Express **25**, 11265–11274 (2017).
3. Y. Shen, X. Wang, Z. Xie, *et al.*, "Optical vortices 30 years on: OAM manipulation from topological charge to multiple singularities," Light Sci. Appl. **8**, 90 (2019).
4. S. M. Barnett, M. Babiker, and M. J. Padgett, "Optical orbital angular momentum," Philos. Trans. R. Soc. A **375**, 20150444 (2017).
5. G. J. Gbur, *Singular Optics* (CRC Press, 2016).
6. F. Gori, M. Santarsiero, R. Borghi, *et al.*, "Partially coherent sources with helicoidal modes," J. Mod. Opt. **45**, 539–554 (1998).
7. S. A. Ponomarenko, "A class of partially coherent beams carrying optical vortices," J. Opt. Soc. Am. A **18**, 150–156 (2001).
8. D. Palacios, I. Maleev, A. Marathay, *et al.*, "Spatial correlation singularity of a vortex field," Phys. Rev. Lett. **92**, 143905 (2004).
9. G. V. Bogatyryova, C. V. Fel'de, P. V. Polyanskii, *et al.*, "Partially coherent vortex beams with a separable phase," Opt. Lett. **28**, 878–880 (2003).
10. M. Padgett and R. Bowman, "Tweezers with a twist," Nat. Photonics **5**, 343–348 (2011).
11. A. Vaziri, J.-W. Pan, T. Jennewein, *et al.*, "Concentration of higher dimensional entanglement: qutrits of photon orbital angular momentum," Phys. Rev. Lett. **91**, 227902 (2003).
12. X.-L. Wang, X.-D. Cai, Z.-E. Su, *et al.*, "Quantum teleportation of multiple degrees of freedom of a single photon," Nature **518**, 516–519 (2015).
13. S. A. Ponomarenko, "Twist phase and classical entanglement of partially coherent light," Opt. Lett. **46**, 5958–5961 (2021).
14. G. Gibson, J. Courtial, M. J. Padgett, *et al.*, "Free-space information transfer using light beams carrying orbital angular momentum," Opt. Express **12**, 5448–5456 (2004).
15. E. Abramochkin and V. Volostnikov, "Generalized Gaussian beams," J. Opt. A **6**, S157 (2004).
16. S. Rasouli, P. Amiri, and D. Hebri, "Transformation of Laguerre-Gaussian beams into 1D array of Hermite-Gaussian modes under the Talbot effect," Opt. Express **31**, 20683–20695 (2023).
17. A. Volyar, E. Abramochkin, Y. Akimova, *et al.*, "Control of the orbital angular momentum via radial numbers of structured Laguerre–Gaussian beams," Opt. Lett. **47**, 2402–2405 (2022).
18. A. Volyar, E. Abramochkin, Y. Akimova, *et al.*, "Super bursts of the orbital angular momentum in astigmatic-invariant structured LG beams," Opt. Lett. **47**, 5537–5540 (2022).
19. V. V. Kotlyar and A. A. Kovalev, "Controlling orbital angular momentum of an optical vortex by varying its ellipticity," Opt. Commun. **410**, 202–205 (2018).
20. A. Nugrowati, W. Stam, and J. Woerdman, "Position measurement of non-integer OAM beams with structurally invariant propagation," Opt. Express **20**, 27429–27441 (2012).
21. V. V. Kotlyar, A. A. Kovalev, and A. P. Porfirev, "Asymmetric Gaussian optical vortex," Opt. Lett. **42**, 139–142 (2017).
22. M. Berry, "Optical vortices evolving from helicoidal integer and fractional phase steps," J. Opt. A **6**, 259 (2004).
23. V. Kotlyar, A. Kovalev, and V. Soifer, "Asymmetric Bessel modes," Opt. Lett. **39**, 2395–2398 (2014).
24. A. Kovalev, V. Kotlyar, and A. Porfirev, "Asymmetric Laguerre-Gaussian beams," Phys. Rev. A **93**, 063858 (2016).
25. D. Hebri and S. Rasouli, "Combined half-integer Bessel-like beams: a set of solutions of the wave equation," Phys. Rev. A **98**, 043826 (2018).
26. V. V. Kotlyar, S. N. Khonina, A. A. Almazov, *et al.*, "Elliptic Laguerre-Gaussian beams," J. Opt. Soc. Am. A **23**, 43–56 (2006).
27. A. Kumar, P. Vaity, and R. Singh, "Crafting the core asymmetry to lift the degeneracy of optical vortices," Opt. Express **19**, 6182–6190 (2011).
28. M. R. Dennis, "Rows of optical vortices from elliptically perturbing a high-order beam," Opt. Lett. **31**, 1325–1327 (2006).
29. V. Kotlyar, A. Kovalev, and A. Porfirev, "Vortex Hermite–Gaussian laser beams," Opt. Lett. **40**, 701–704 (2015).
30. V. Kotlyar, A. Kovalev, and A. Porfirev, "Elliptic Gaussian optical vortices," Phys. Rev. A **95**, 053805 (2017).
31. D. Hebri, S. Rasouli, and A. M. Dezfouli, "Theory of diffraction of vortex beams from structured apertures and generation of elegant elliptical vortex Hermite–Gaussian beams," J. Opt. Soc. Am. A **36**, 839–852 (2019).
32. D. Zwillinger and A. Jeffrey, *Table of Integrals, Series, and Products* (Elsevier, 2007).
33. B. E. Saleh and M. C. Teich, *Fundamentals of Photonics* (Wiley, 2019).
34. J. D. Gaskill, *Linear systems, Fourier Transforms, and Optics* (Wiley, 1978), Vol. **56**.
35. S. Khonina, V. Kotlyar, V. Soifer, *et al.*, "An analysis of the angular momentum of a light field in terms of angular harmonics," J. Mod. Opt. **48**, 1543–1557 (2001).